Bio-Design and Manufacturing (2024) 7:153–166
https://doi.org/10.1007/s42242-023-00267-x

RESEARCH ARTICLE

Dissolvable temporary barrier: a novel paradigm for flexible hydrogel patterning in organ-on-a-chip models

Ding Wang[1] · Qinyu Li[2] · Chenyang Zhou[1] · Zhangjie Li[1] · Kangyi Lu[1] · Yijun Liu[1] · Lian Xuan[3] · Xiaolin Wang[1,3,4,5]

Received: 10 August 2023 / Accepted: 24 December 2023 / Published online: 23 February 2024

Abstract

A combination of hydrogels and microfluidics allows the construction of biomimetic three-dimensional (3D) tissue models in vitro, which are also known as organ-on-a-chip models. The hydrogel patterning with a well-controlled spatial distribution is typically achieved by embedding sophisticated microstructures to act as a boundary. However, these physical barriers inevitably expose cells/tissues to a less physiologically relevant microenvironment than in vivo conditions. Herein, we present a novel dissolvable temporary barrier (DTB) strategy that allows robust and flexible hydrogel patterning with great freedom of design and desirable flow stimuli for cellular hydrogels. The key aspect of this approach is the patterning of a water-soluble rigid barrier as a guiding path for the hydrogel using stencil printing technology, followed by a barrier-free medium perfusion after the dissolution of the DTB. Single and multiple tissue compartments with different geometries can be established using either straight or curved DTB structures. The effectiveness of this strategy is further validated by generating a 3D vascular network through vasculogenesis and angiogenesis using a vascularized microtumor model. As a new proof-of-concept in vasculature-on-a-chip, DTB enables seamless contact between the hydrogel and the culture medium in closed microdevices, which is an improved protocol for the fabrication of multiorgan chips. Therefore, we expect it to serve as a promising paradigm for organ-on-a-chip devices for the development of tumor vascularization and drug evaluation in the future preclinical studies.

Graphic abstract

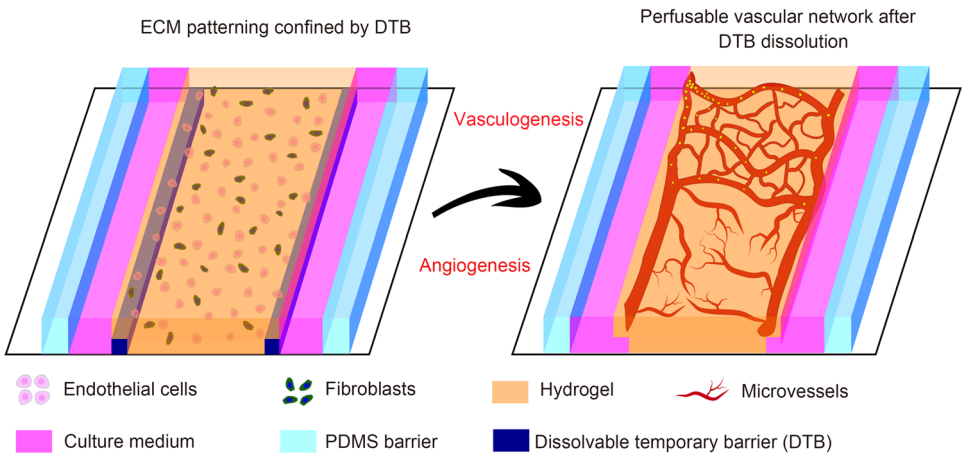

Keywords Dissolvable temporary barrier · Hydrogel patterning · Microfluidics · Organ-on-a-chip · Vascularization

Ding Wang and Qinyu Li have contributed equally to this work.

Extended author information available on the last page of the article

Introduction

Organ-on-a-chip technology has attracted substantial interest because of its advantages in simulating the three-dimensional (3D) microstructures and neurophysiological functions of human tissue, and it shows great potential for drug discovery and disease modeling [1–4]. Microfluidic technologies are useful tools that can precisely recapitulate many features of an in vivo microenvironment, such as different profiles of fluid flow or the concentration gradient of specific growth factors [5]. Meanwhile, hydrogel as a scaffold can simulate the porosity and tissue elasticity of the extracellular matrix (ECM). The majority of perfusion-based organ-on-a-chip devices have been established because of the nutrient supply and waste product removal requirements of long-term microtissue coculture [6–8]. One of the most popular methods for achieving sought-after ECM patterning is filling the central tissue culture chamber with an adjacent hydrogel, followed by the perfusion of medium into two-sided microchannels [9]. Because the geometries of patterned ECM determine the interstitial flow rate that directly stimulates of cell/tissue growth, fulfilling the robust and flexible ECM patterning with high spatial resolution is crucial to the construction of an on-chip dynamic microenvironment.

Currently, a variety of physical barriers are used as pattern boundaries, such as micropillar arrays and phaseguide microstructures [10–13]. Through abrupt changes in either channel geometry or hydrophilicity, these barriers can function as capillary burst valves to form high-energy menisci after hydrogel perfusion [14, 15]. However, the contact area is inevitably reduced, and air bubbles are likely to be trapped between the medium and ECM, eventually affecting cell behavior in undesirable ways. Moreover, the unsatisfactory integrity of the monolayer along the ECM–medium interface would result in a poor basement membrane, especially for tissue coculture between the parenchymal and vascular sides. Therefore, temporary or virtual barriers are required for a more reliable ECM confinement without the use of additional physical microstructures.

Laminar flow is another approach that is utilized to separate one microchannel into multiple subchannels using hydrogel micro-slabs [16]. However, this method relies heavily on accurate flow control and the specific properties of hydrogels (e.g., viscosity and thermal curing properties). Although the width of the hydrogel can be adjusted, local surface modification is required to create a hydrophilic microfluidic channel for ECM patterning [17]. Laminar flow allows ECM patterning inside long straight and curved structures; however, it is limited by the geometry of the microfluidic channel. Another strategy is to establish a transient compartment by embedding the cylindrical microfilaments as the guiding structures, followed by the removal of the microfilaments after gel polymerization with minimal hydrodynamic perturbation [18]. However, this method is only suitable for building regular straight tissue chambers. In addition, a thin nanoporous membrane constructed by the interfacial polymerization reaction at the interface between the two reagents could be used as a removable barrier. For example, the reaction between a buffer solution and an acidic chitosan solution could generate a chitosan membrane, which could then be removed by flushing the acidic solution [19]. To construct a stable interface, both the pH and flow rate must be precisely regulated. However, a temporary membrane with complex structures would be difficult to fabricate using this method. The idea of using a pneumatic valve as an alternative was recently proposed to establish a recoverable elastic barrier, separating the chamber into single or multiple compartments with either regular or irregular structures [20]. However, the fabrication process was time-consuming and required excellent alignment between multiple layers. Moreover, external fluidic control equipment such as the air pump was required for the actuation of the elastic barrier.

In this study, we present a novel dissolvable temporary barrier (DTB) design that achieves robust ECM patterning without hydrogel bursting or leaking. Notably, a DTB can be dissolved shortly after the culture medium is injected, and the physiological flow stimuli to the cells/tissues can be improved inside the ECM. The effectiveness of this method is validated by its application to different microfluidic devices for the reconstruction of vascularized microtissues. Compared with previous ECM patterning methods, the DTB design exhibits multiple beneficial features, including (1) simple and flexible DTB patterning through stencil printing; (2) robust ECM loading into single or multiple culture compartments without leakage; (3) free interface without physical obstacles for improved flow stimulation; (4) a barrier-free imaging window and multitissue coculture with an intact basement membrane; (5) spontaneous barrier dissolution after medium perfusion without chemical reactions or the need for external equipment; and (6) high compatibility with versatile organ-on-a-chip designs. Therefore, we expect this to be a promising paradigm for the development of versatile in vitro organ-on-a-chip models toward a more physiologically relevant microenvironment.

Materials and methods

Chip design and fabrication

Figure 1 shows a schematic design and the fabrication process for a microfluidic chip with a DTB, including a top microchannel-embedded layer and a bottom glass substrate with the DTB. A polyvinyl alcohol (PVA)-based DTB was patterned on a glass substrate using screen printing (Fig. 1a). Briefly, a stainless steel sheet with a thickness of 120 μm was

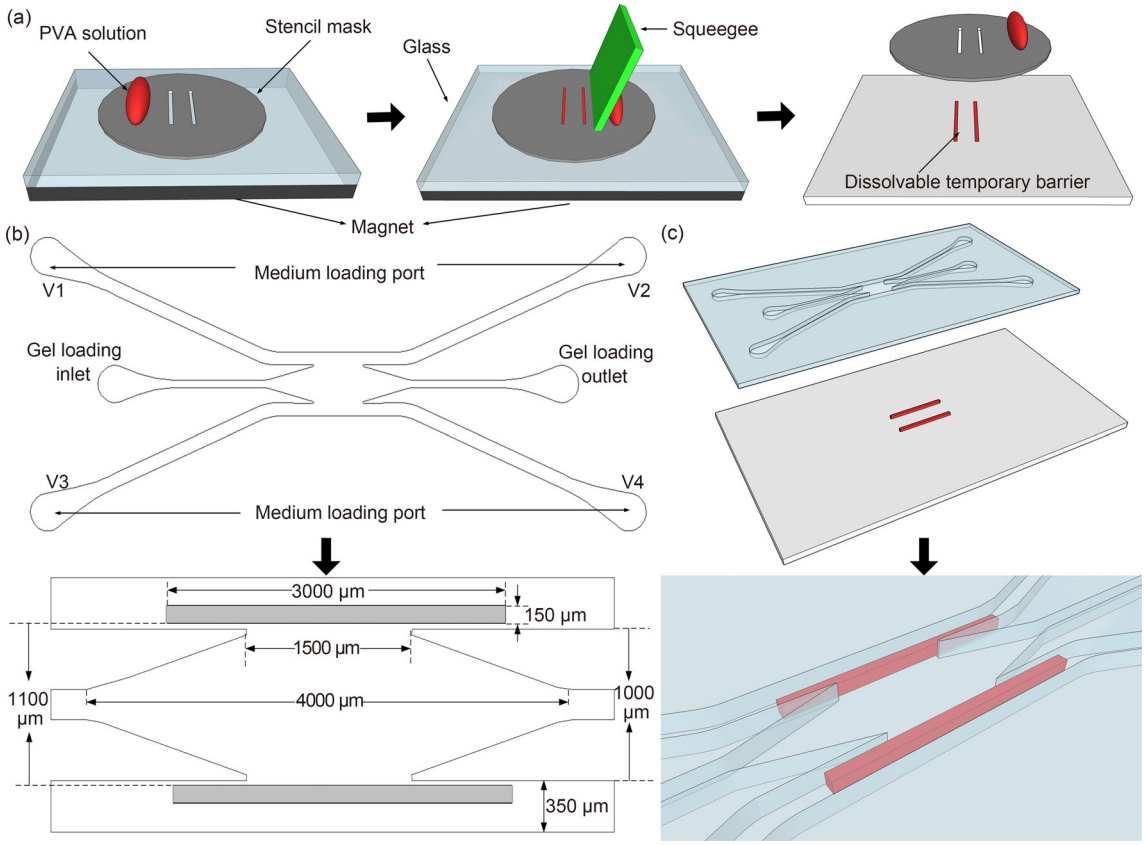

Fig. 1 Schematic design and fabrication of microfluidic chip with DTB. **a** Microfabrication of DTB by screen printing using a PVA solution. **b** Microstructure of the overall design and corresponding structural parameters. **c** Schematic illustration of two layers before bonding, and magnified view of the tissue chamber after assembly. DTB: dissolvable temporary barrier; PVA: polyvinyl alcohol

first processed into a stencil mask with two strip-shaped hollow structures (length×width: 3000 μm×150 μm) by laser cutting. To prevent PVA leakage during printing, a stencil mask was closely attached to the sandwiched glass substrate using a magnet. A PVA solution with high viscosity was subsequently used to fill the open mesh with a squeegee, and the solution was then solidified after 7 min at 60 °C. After PVA curing, the stencil mask was detached from the glass substrate without damaging the DTB. It should be noted that as a proof-of-concept, the stencil mask was also designed with various hollow shapes to meet practical requirements (Fig. S1 in Supplementary Information).

The microfluidic chip consisted of one central tissue chamber (length×width: 4000 μm×1000 μm) with two gel loading ports and two microfluidic channels (width×length: 350 μm×200 μm) on the side with a total of four medium loading ports (Fig. 1b). No physical barriers, such as a micropillar array or a phaseguide structure, were present. Instead, a large opening with a width of 1500 μm was positioned between the tissue chamber and the microfluidic channels. The height of the chamber was 200 μm, which was nearly twice the thickness of the DTB after curing. The top microfluidic layer was made of polydimethylsiloxane (PDMS) (Sylgard-184, Dow Corning, USA) using standard soft lithography techniques. After holes were punched in the top layer for the gel and the medium was loaded, the top layer with microchannels was well aligned; it was bonded to the glass substrate with a DTB using oxygen plasma treatment (Fig. 1c). To facilitate manual alignment under a microscope, the gap (1100 μm) between the two DTBs was designed to be slightly larger than the width (1000 μm) of the tissue chamber. Furthermore, to increase the redundancy of the alignment, the length of the DTB (3000 μm) was designed to be larger than the width of the opening (1500 μm).

Principle of DTB design

The entire gel loading process could be compared with an electric circuit model (Fig. 2a) [12]. The externally applied pressure (P_{appl}) for gel loading and the capillary pressure (P_{cap}) at the gel–air interface are analogous to the direct current (DC) voltage source. The inverted diode represents the DTB, and its breakdown level corresponds to the overflow pressure ($P_{overflow}$). The electric resistances R_1 and R_2 are

analogous to the hydraulic resistances located at the rear and front sides of the DTB–gel interface, respectively. Therefore, pressure P along the DTB–gel interface inside the tissue chamber can be defined as follows:

$$P = \frac{R_2}{R_1 + R_2}\left(P_{\text{appl}} + P_{\text{cap}}\right) - P_{\text{cap}}. \quad (1)$$

Pressure P increases with either externally applied pressure or gel advancement inside the tissue chamber. Thus, to achieve robust hydrogel loading without bursting the gel near the DTB, the following conditions must be satisfied:

$$P_{\text{advancing}} < P < P_{\text{overflow}}. \quad (2)$$

Here $P_{\text{advancing}}$ represents the pressure required for gel movement when the contact angles between the gel and all sidewalls exceed the critical advancing contact angle, which can be expressed by the Young–Laplace equation as follows [15]:

$$P_{\text{advancing}} - P_{\text{air}} = -2\gamma(\cos(\theta_s/w) + \cos(\theta_v/h)). \quad (3)$$

Here P_{air} represents the atmospheric pressure, γ is the surface tension, w and h are respectively the width and height of the tissue chamber where the interface is located, θ_s is the critical advancing contact angle between the gel interface and the sidewalls, and θ_v is the critical advancing contact angle between the gel interface and the top/bottom walls.

However, if the pressure of the meniscus pinned at the DTB increases above a certain value, P_{overflow}, the gel will burst into the side microchannels. The value of P_{overflow} can be described using the Concus–Finn criterion [21]:

$$\alpha_{\text{crit}} = 180^\circ - (\theta_1 + \theta_2). \quad (4)$$

Here α_{crit} is the critical angle for the fully stretched meniscus, θ_1 is the contact angle between the meniscus and the top microfluidic wall, and θ_2 is the contact angle between the meniscus and the bottom DTB. For a DTB with a vertical sidewall, θ_1+θ_2 should be larger than 90° for complete pinning regardless of the height of the DTB (Fig. 2b). In other words, the meniscus climbs the front of the DTB and walks on it. Finally, the meniscus would be pinned at the back edge of DTB, thereby stopping the overflow.

When the DTB is with a sufficient height, the meniscus will be pinned at the front of the DTB. In this case, the Concus–Finn criterion would no longer be applicable [22]. Therefore, to prevent gel overflow across the DTB during the loading process, either a large contact angle with the solid surface or a sufficiently high DTB is crucial.

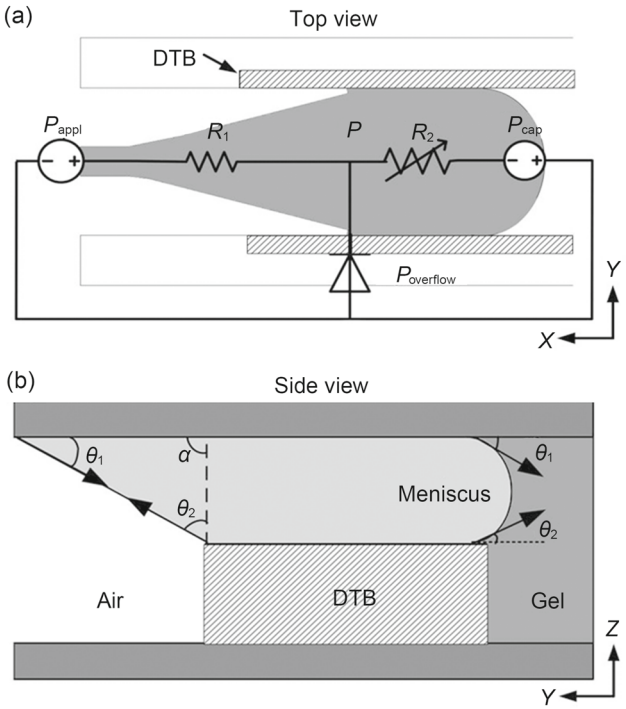

Fig. 2 Principle of DTB design. **a** Schematic of simplified electric circuit model with DTB design during the gel loading process. **b** Meniscus-pinning effect along DTB based on Concus–Finn criterion. DTB: dissolvable temporary barrier

Finite element simulation

A finite element simulation was performed using COMSOL Multiphysics 5.4a (Comsol Inc., Burlington, MA, USA). For the simulation of the interstitial flow across a patterned ECM inside the tissue chamber, the Brinkman equation from the Chemical Engineering Module was employed for momentum transportation through a porous hydrogel, with parameters of low permeability (1.5×10^{-13} m^2) and high porosity (0.99). The high-pressure area was defined to be inside the top microfluidic channel (V1: 196 Pa; V2: 117.6 Pa), and the low-pressure area was defined to be inside the bottom microfluidic channel (V3: 117.6 Pa; V4: 39.2 Pa). Thus, the hydrostatic pressure drop across the tissue chamber was set to 8 mmH_2O (i.e., 78.4 Pa) as previously described [14, 23]. No-slip boundary conditions were applied to the other walls. An extremely fine mesh size was used to achieve high accuracy. All the parameters used in the simulation are listed in Table S1 (Supplementary Information).

To simulate the flow profile inside the vessel lumen of the formed microvascular network, the incompressible Navier–Stokes equation in the micro-electro-mechanical system (MEMS) module was utilized, and the media flow was set to a density of 1000 kg/m^3 and a dynamic viscosity of 1×10^{-3} Pa·s. To extract the structure of the microvascular network, a two-dimensional fluorescent image of the

microvessels was first binarized using ImageJ (National Institutes of Health, USA). This was followed by image processing to remove different types of noise, such as image dilation and erosion. Then, the contour profile was processed using an edge detection algorithm and converted to a vectorized file (such as a DFX file) using Img2CAD software (Version 7.3, Cologne, Germany). The vector file was then imported into COMSOL. Similarly, the top boundary of the microvascular network was set as an inlet with a hydrostatic pressure of 78.4 Pa, and the outlet pressure of the bottom boundary was set to 0.

PVA solution preparation

A PVA solution with high viscosity (44–56 mPa·s) was prepared by mixing medical class PVA powder with a purity of 97% (Shanghai Chenqi Chemical Technology Co., Ltd., China) in purified water at a mass ratio of 1:5. Typically, PVA has a high solubility with a large mesh number. In this study, the mesh number of the selected PVA powder was 120; thereby, the powder could be easily dissolved, even in cold water. After the powder was fully stirred and dissolved, the PVA solution was placed in a vacuum chamber to remove the air bubbles. The degassed PVA solution was then used to form the DTB by screen printing.

Cell culture and ECM preparation

For cell/tissue culture and ECM preparation, all experimental procedures were performed using sterile techniques inside a Biosafety Level 2 laminar flow hood. Human endothelial colony-forming cell-derived endothelial cells (ECFC-ECs) were isolated from cord blood and cultured in Endothelial Cell Growth Medium-2 (EGM-2, Lonza, Switzerland) as previously described [24, 25]. The ECFC-ECs were then transfected with lentivirus constructs (Addgene, USA) to express a red fluorescent protein (RFP), and ECFC-ECs were used between Passages 5–7. Normal human lung fibroblasts (NHLFs) (Lonza) cultured in Fibroblast Growth Medium-2 (FGM-2, Lonza, Switzerland) were used between Passages 5–8. Human glioblastoma cells (U87MG) (Cell Bank of Shanghai Bioscience Center, Chinese Academy of Sciences) were cultured in Dulbecco's modified Eagle medium (DMEM, Gibco, USA) supplemented with 10% fetal bovine serum (Gibco, USA) and 1% penicillin–streptomycin (Gibco, USA). All cells were cultured in an incubator at 37 °C and 5% CO_2.

Bovine fibrinogen (Sigma-Aldrich, USA) and bovine thrombin (Sigma-Aldrich) were separately dissolved in Dulbecco's phosphate-buffered saline (DPBS, Gibco, USA) to produce a 10 mg/mL fibrinogen solution and a 10 U/mL bovine solution. After the cells were harvested, ECFC-ECs (1×10^7 cells/mL) and NHLFs (1×10^7 cells/mL) were mixed and resuspended in fibrinogen solution. Cellular fibrinogen solution was aspirated and mixed with bovine thrombin for polymerization. This was followed by the injection of the solution into the tissue chamber. Before the experiments, all chips were sterilized under ultraviolet radiation for 2 h.

Fluidic flow control

Interstitial flow across the ECM inside the tissue chamber and shear stress along the microfluidic channels are the dominant biomechanical factors. To maintain a physiological level of interstitial flow velocity for vasculogenesis within the optimal range (0.1–11 μm/s), an initial hydrostatic pressure drop of 8 mmH_2O was established by filling the medium reservoirs to different heights (V1: 20 mmH_2O; V2: 12 mmH_2O; V3: 12 mmH_2O; V4: 4 mmH_2O). Because the hydrostatic pressure across the hydrogel decreased over time, the liquid level had to be manually restored to its initial value every day. In addition, to stimulate the cells with symmetrical pressure gradients, the flow direction was switched every two days (V1: 12 mmH_2O; V2: 4 mmH_2O; V3: 20 mmH_2O; V4: 12 mmH_2O). The culture medium was replaced every alternate day.

Imaging and analysis

Fluorescent images were captured using an Olympus CKX53 inverted microscope with a high-resolution camera (BioHD-A16c, FluoCa Scientific Pte. Ltd., Singapore). Images from different fluorescence channels were overlapped using ImageJ software. Confocal imaging was performed using a Leica TCS SP8 STED 3X camera (Leica Microsystems, Germany). The images were stitched together manually to obtain panoramic vessel images inside entire tissue chambers. To characterize the vascular network, the total vessel area/length and the number of junctions were measured using AngioTool software (National Institutes of Health, USA), followed by a statistical analysis using GraphPad Prism.

Results

ECM patterning confined by DTB

Figures 3a and 3b show a visible screen-printed DTB on a glass substrate, blocking the large opening of a tissue chamber after plasma bonding. Although the thickness of the DTB being almost half the height of the tissue chamber, ECM was desirably confined along the patterned DTB without bursting into the side microfluidic channels because of the meniscus-pinning effect. The success rate of ECM patterning could be improved by regulating the height of the stencil mask or by

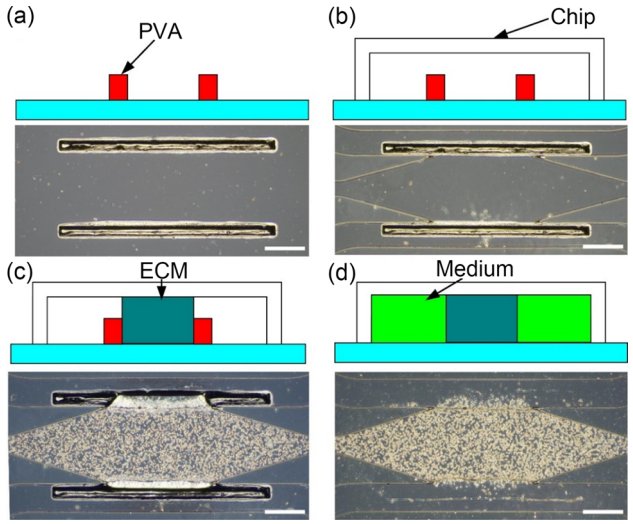

Fig. 3 Schematic and experimental results of ECM patterning from the top view. **a** DTB patterning through stencil printing. **b** Microfluidic chip with DTB after bonding. **c** ECM patterning without bursting and partially solubilized DTB after contact with hydrogel. **d** Completely dissolved DTB after medium perfusion. Scale bar: 300 μm. ECM: extracellular matrix; DTB: dissolvable temporary barrier; PVA: polyvinyl alcohol

performing multiple overlapping printings (Fig. S2 in Supplementary Information). Owing to the high water content of the hydrogel, the DTB was partially dissolved 2 min after it came into close contact with the hydrogel (Fig. 3c); 2 min is much longer than the time required for gel polymerization (approximately 20 s). Therefore, the ECM patterning inside the tissue chamber was not affected by the dissolution of DTB. After perfusion of the culture medium, the DTB was completely dissolved within 20 min, and then, a large contact area was formed between the ECM and medium (Fig. 3d). Robust and desirable ECM patterning without bursting could eventually be achieved in the form of a nonphysical barrier.

Finite element simulation of the interstitial flow

To demonstrate the advantages of DTB design over other physical barrier designs, such as the micropillar array, finite element simulations of the pressure distribution and the interstitial flow rate inside the ECM were performed. In the DTB design, the pressure across the ECM was linearly distributed along the vertical direction under a hydrostatic pressure drop of 8 mmH_2O (Figs. 4a and 4b).

However, in the micropillar array design (Fig. 4c), because only a portion of the medium between the adjacent micropillars flows into the hydrogel, a nonuniform pressure distribution was observed under high fluidic resistance. Correspondingly, the interstitial flow velocity in the middle of the tissue chamber along the horizontal direction in the DTB design (9.95–15.7 μm/s) was two to three times larger than that for the micropillar array design (4.8–6.21 μm/s) (Fig. 4d). Thus, fluidic stimulation to cells in the DTB design became preferable to the micropillar array design under a given hydraulic pressure. To visualize the pressure distribution during the perfusion of the medium in these two designs, 70-kDa fluorescein isothiocyanate-dextran (FITC-dextran) was loaded into the side microfluidic channels. The pressure-induced diffusion of dextran was observed across the whole tissue chamber within 3 min in the DTB design, which was much faster than the diffusion in the micropillar array design (Movie S1 in Supplementary Information). These results indicate that the use of an appropriate hydrostatic pressure stimulation made it possible to reconstruct a similar physiological environment in the DTB design.

Vasculogenesis after DTB dissolution

After injecting the ECM and establishing interstitial flow inside the tissue chamber, RFP-labeled ECFC-ECs formed vascular fragments on Day 1 and developed into a capillary network on Day 5 (Fig. 5 and Movie S2 in Supplementary Information). By Day 9, the capillary network was further lumenized and interconnected between two-sided microfluidic channels. Interestingly, ECs would migrate outward to the microfluidic channels to form a confluent monolayer near the gel interface. This monolayer anastomosed with the capillary network inside the tissue chamber and constructed an intact microvascular network. Furthermore, the blood vessels became much denser, with an enlarged lumen size on Day 13. More importantly, the distribution and size of the lumen were unrestricted because of the large opening between the tissue chamber and microfluidic channels, which would better recapitulate the anastomosed capillary network with good perfusion capacity in vivo.

Figure 6 shows a comparison of vascularization between the micropillar array and DTB design, whose tissue chambers were of the same size. Unlike the micropillar array design, vascular fragments in the DTB design were already anastomosed into the microvascular network on Day 6. As shown in Fig. 6c, the total vessel area in the DTB design (1.53×10^6 μm^2) was almost twice as large as that in the micropillar array design (7.9×10^5 μm^2). Correspondingly, the total vessel length and number of junctions in the DTB design were 3.75×10^4 μm and 181, respectively, which were significantly larger than those of the micropillar array design (2.72×10^4 μm and 112, respectively). These experimental results confirm that the DTB design provides sufficient fluidic stimuli to the cells/tissues, and the results are correlated with the corresponding simulation results.

The DTB was also compatible with other chamber structures having great freedom of design, such as the two interconnected diamond-shaped tissue chambers (Fig. 7). Notably, the structure of the microvascular network tended

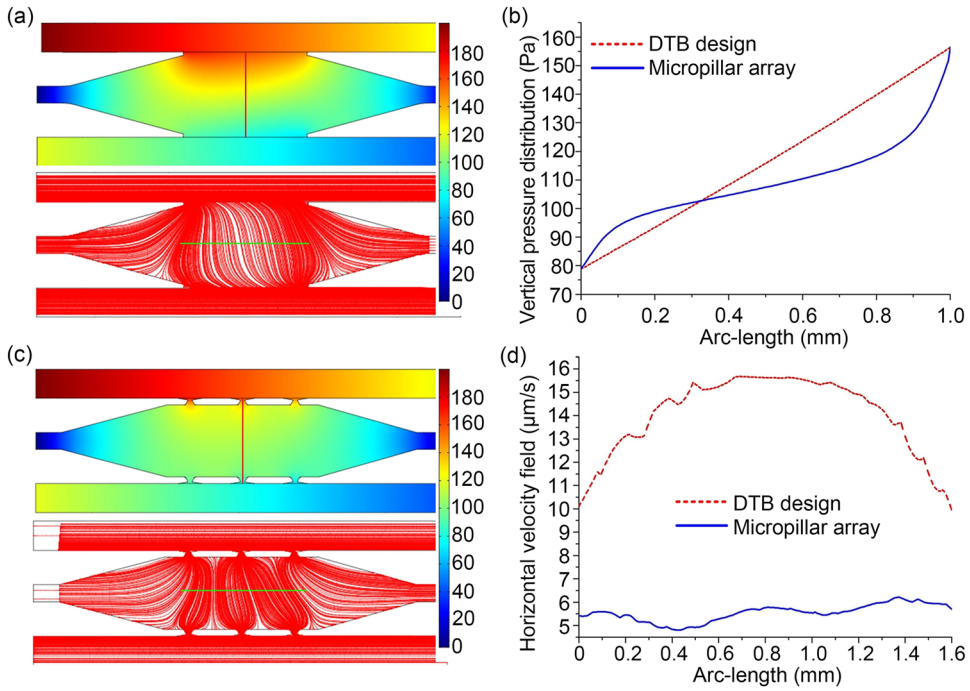

Fig. 4 Simulation results for pressure distribution and interstitial flow profile inside ECM confined by DTB and micropillar array. **a** Pressure distribution and flow streamline for DTB design. **b** Vertical pressure distribution for DTB and micropillar array designs. **c** Pressure distribution and flow streamline for micropillar array design. **d** Horizontal velocity field for DTB and micropillar array designs. ECM: extracellular matrix; DTB: dissolvable temporary barrier

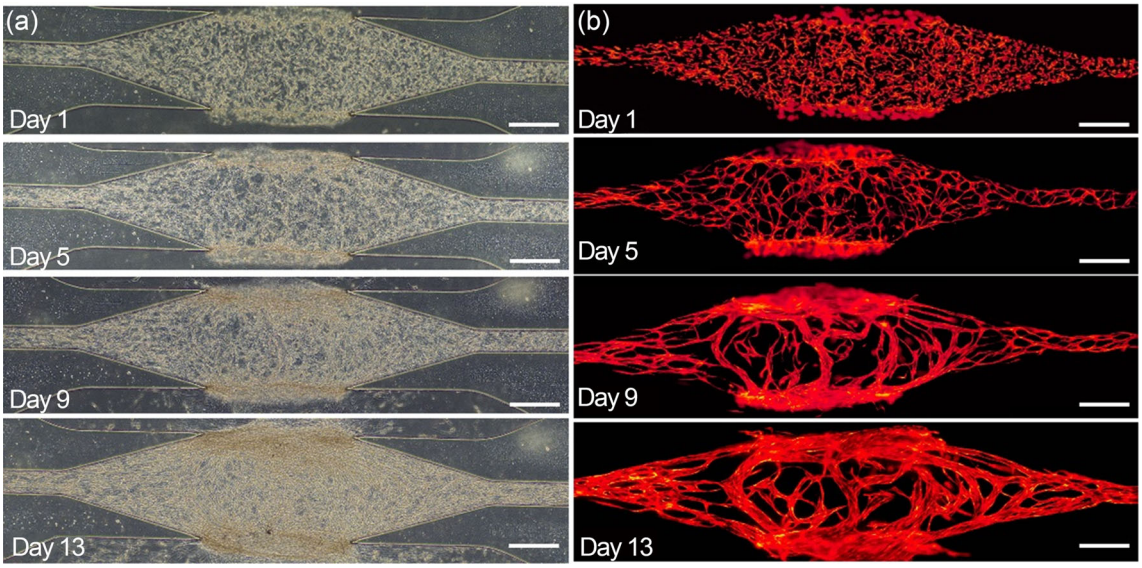

Fig. 5 Process of vasculogenesis inside a tissue chamber over 13 days. **a** Bright-field and **b** fluorescent images of the vascular network. Scale bar: 400 μm

to be consistent with the flow streamlines inside the tissue chamber, especially in areas where two tissue chambers were interconnected (Fig. 7a). This result further proves that the mechanical stimuli of shear stress would enhance EC alignment along the flow direction by mechanotaxis, which is critical in vascular remodeling [26]. Additionally, vascular networks in tissue chambers with different sizes and opening dimensions could be created (Fig. 7b) and further utilized to study different organs. Furthermore, the fiber arrangements inside an ECM would affect vessel alignment in response to contact guidance under different geometrical shapes of the chamber [27]. The orientation of the fibrils could be flexibly regulated along the flow direction by changing the aspect ratio of the tissue chamber (Fig. 7c), which demonstrates that the DTB design enables specific vascular arrangements.

Perfusion capacity of the microvascular network

Confocal imaging was performed to demonstrate the 3D vascular distribution at different heights within a thickness

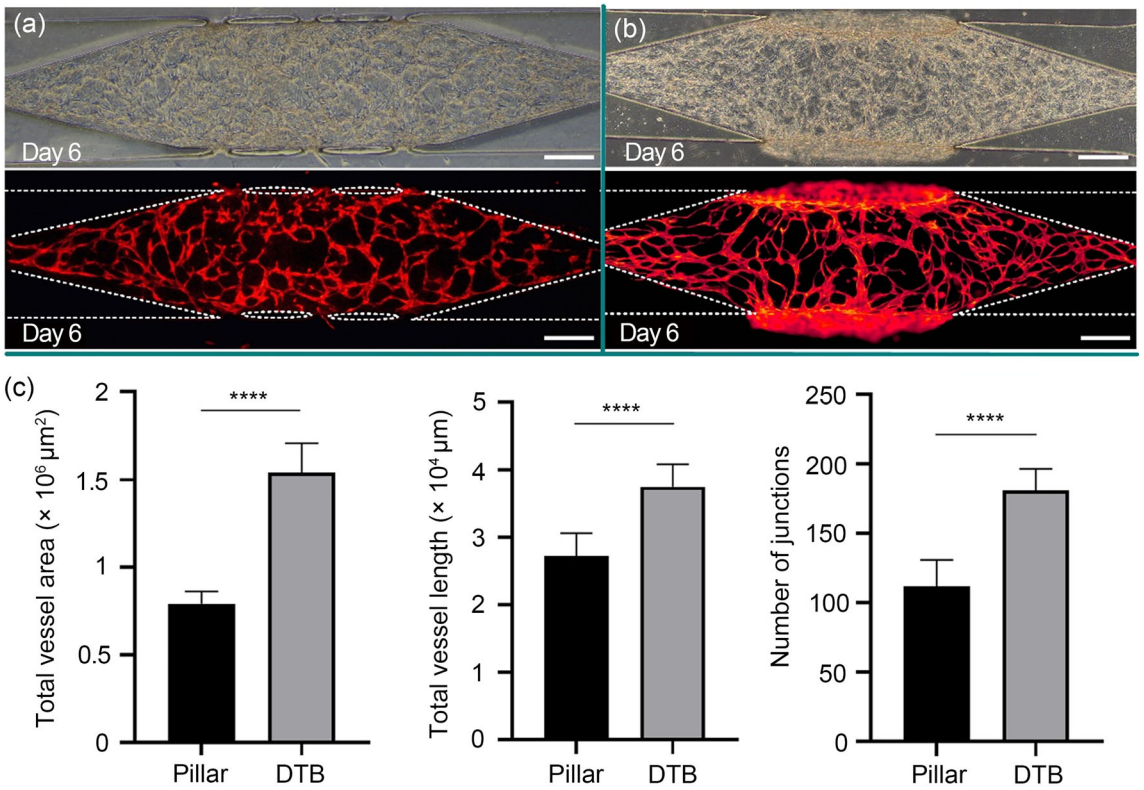

Fig. 6 Comparison of vascularization between micropillar array and DTB design. **a** Bright-field and fluorescent images of noninterconnected vascular fragments in micropillar array design. Scale bar: 400 μm. **b** Bright-field and fluorescent images of the anastomosed microvascular network in DTB design. Scale bar: 400 μm. **c** Quantitative analysis of total vessel area, total vessel length, and number of junctions in two different designs (mean±standard deviation, n=8, $^{****}p$<0.0001, unpaired two-tailed Student's t-test). DTB: dissolvable temporary barrier

of 180 μm in the tissue chamber (Fig. 8a and Movie S3 in Supplementary Information). In addition, both the horizontal (X-Y plane) and vertical (X-Z plane and Y-Z plane) cross-sectional images showed that vessel branches formed hollow lumens with a diameter of approximately 25 μm (Fig. 8b). To confirm the perfusion capacity of the vascular network, fluorescent microparticles with a diameter of 5 μm were introduced into the side microfluidic channel under high hydrostatic pressure. These microparticles flowed through the vascular lumens into the opposite channel with minimal adherence to the vessel wall (Fig. 8c and Movie S4 in Supplementary Information). Similarly, red blood cells from mice traversed through the vascular network in the tissue chamber without leakage (Movie S5 in Supplementary Information). To further evaluate vascular permeability, 70-kDa FITC-dextran was injected into the microchannel. Owing to the pressure gradient, the influx of dextran into the vascular network could easily be observed, and no dextran flowed outside the vessel lumens within 10 min after perfusion (Fig. 8d and Movie S6 in Supplementary Information). Additionally, ECs that highly expressed cluster of differentiation 31 (CD31) tightly adhered to each other in the vascular network (Fig. 8e). These results demonstrate the excellent transport ability of the vasculature and desirable barrier functions of the vessel walls.

To further study the microphysiological environment of the engineered vascular network, a simulation of the flow velocity and shear stress inside the vessel lumens was performed (Fig. 8f) based on the vascular morphology at Day 13 in Fig. 5. The maximum and average flow velocities inside the vessel lumens were 330 and 27.65 μm/s, respectively. The flow velocity increased with a larger lumen size, owing to the lower flow resistance. Similarly, the maximum and average shear stresses along the lumen walls were 156.6 and 3.77 dyne/cm^2, respectively. These results were in accordance with the microphysiological environment of the human capillary network in vivo and contribute to a better understanding of how flow and shear influence vessel remodeling [28].

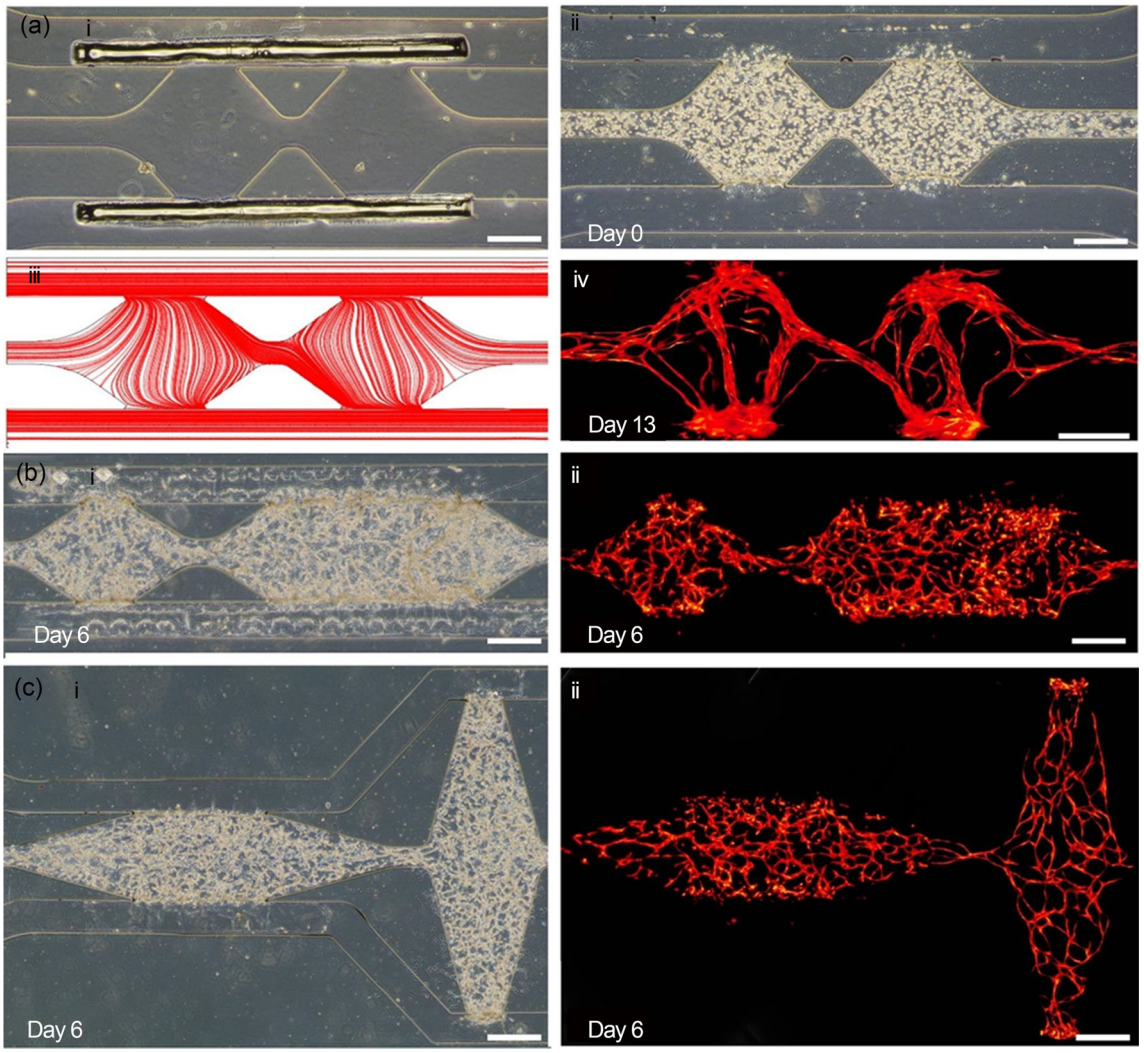

Fig. 7 Vascularization inside double-tissue chambers having different geometries and DTB designs. **a** Images of two identical interconnected chambers after (i) plasma bonding, (ii) gel patterning, (iii) streamline simulation, and (iv) vasculogenesis. Scale bar: 400 μm. **b** Images of a vascular network under (i) bright-field and (ii) fluorescence microscope in two interconnected chambers having different sizes and opening dimensions. Scale bar: 500 μm. **c** Images of a vascular network under (i) bright-field and (ii) fluorescence microscope in two interconnected chambers having different aspect ratios. Scale bar: 700 μm. DTB: dissolvable temporary barrier

Angiogenesis from lined EC monolayer at the gel interface

Angiogenesis, a fundamental mechanism of vascular modeling, refers to the growth of new blood vessels from pre-existing vasculature due to an angiogenic stimulus, followed by sprouting, elongation, branching, lumen formation, and anastomosis [29]. In the DTB design, fibrin gel mixed with NHLFs was first perfused into the central tissue chamber confined by the DTB. After polymerization of the gel, a cell culture medium was injected into the two-sided microfluidic channels to completely dissolve the DTB (Fig. S3 in Supplementary Information). The RFP-labeled ECFC-ECs were loaded at a density of 1×10^7 cells/mL into a microfluidic channel. By tilting the chip at an angle of 60° inside the incubator for 30 min, we enabled the ECs to closely attach to the fibrin gel interface. The same operation was performed for the other microfluidic channel. After one day of incubation, visible confluent endothelial monolayers formed on both sides (Fig. 9).

By applying basal-to-apical transendothelial flow, we observed that the lined ECs invaded the fibrin gel and formed angiogenic sprouts on Day 3. Because angiogenic sprouting was only promoted in the direction opposite to the interstitial flow, the direction of fluid flow was switched every two days to allow symmetrical angiogenesis from both sides [30]. On Day 5, highly branched and abundant sprouts further extended into the gel, which

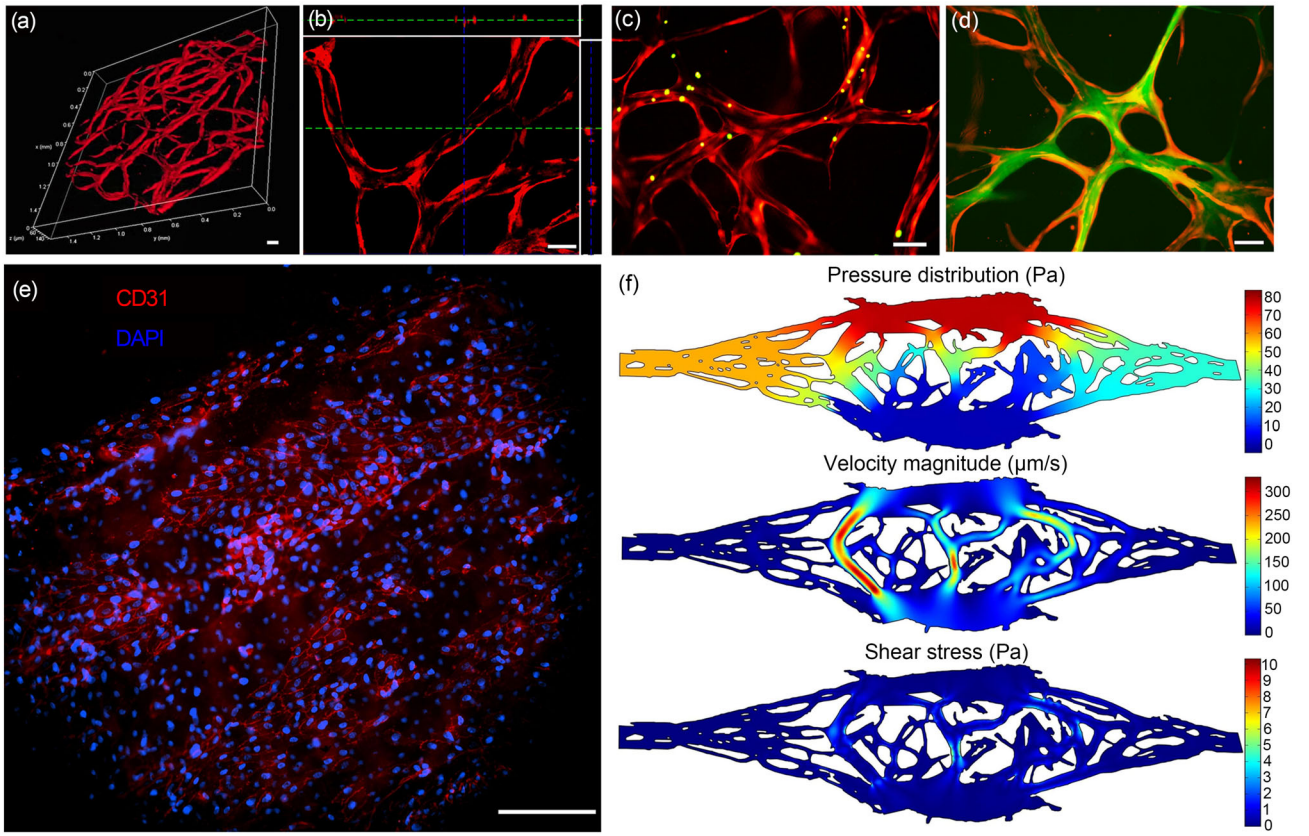

Fig. 8 Perfusion capacity of the 3D microvascular network after vasculogenesis. **a** Confocal image of 3D microvascular network. **b** Magnified image of microvascular network with hollow lumens. **c** Confocal image of perfusion with 5-μm fluorescent microparticles. **d** Fluorescent image of vascular branches at 10 min after the perfusion of 70-kDa FITC-dextran. **e** Merged image of microvascular network immunostained with the endothelial cell adhesion protein CD31 (red), and the nuclei were immunostained with DAPI (blue). **f** Simulation results for pressure distribution, flow velocity, and shear stress inside the vessel lumens. Scale bar: 50 μm. 3D: three-dimensional; FITC-dextran: fluorescein isothiocyanate-dextran; CD31: cluster of differentiation 31; DAPI: 4',6-diamidino-2-phenylindole

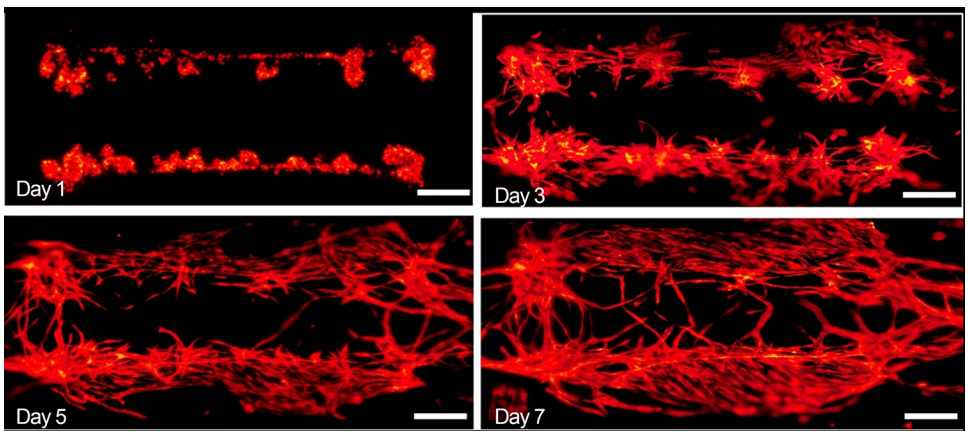

Fig. 9 Angiogenesis process from lined EC monolayers at the gel interface 7 d after perfusion of the gel and cells. Scale bar: 400 μm. EC: endothelial cell

provided the precondition for anastomosis on Day 7. The sprouting branches in the DTB device randomly invaded the ECM and became uniformly distributed in the chamber, rather than remaining in the gap between two adjacent micropillars [14]. In addition, ECs wrapped around the inner surface of the two microchannels, and vessel interconnections from these sprouting branches eventually formed.

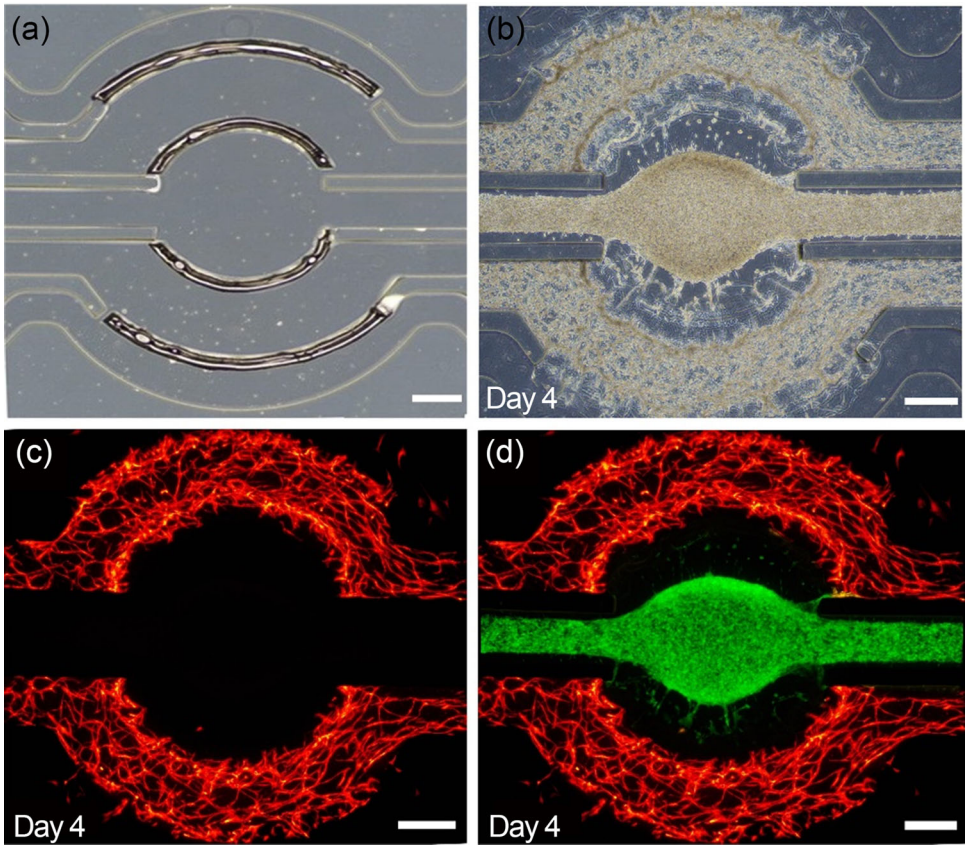

Fig. 10 Construction of vascularized microtumor model with multiple DTBs. **a** Circular tissue chamber is divided into three compartments with four DTBs. **b** Bright-field image after ECM patterning (U87MG in the central chamber; ECs and NHLFs in two side channels). **c** Fluorescence image of vascularization inside half-ring-shaped tissue chambers. **d** Merged fluorescence image of the vascularized microtumor tissue. Scale bar: 400 μm. DTBs: dissolvable temporary barriers; ECM: extracellular matrix; U87MG: human glioblastoma cells; ECs: endothelial cells; NHLFs: normal human lung fibroblasts

Construction of vascularized microtumor model

A majority of the previous studies have reported that cultured microtissues (e.g., tumor spheroids) were either randomly distributed in the microvascular network or spatially confined by physical barriers [24, 31]. Due to the flexibility of the DTB design, both controllable distribution and barrier-free connection of different ECMs can easily and robustly be achieved for multitissue cocultures inside different compartments. As a proof-of-concept, three compartments were designed using four DTBs (Fig. 10). The fibrin gel with RFP-labeled ECFC-ECs and NHLFs was injected into the upper and lower half-ring-shaped tissue chambers. Then, the central circular chamber was patterned with the green fluorescent protein (GFP)-labeled U87MG in the fibrin gel. After 4 d of coculture, the central U87MG microtumor tissue sandwiched by the microvascular network collectively migrated toward the side microvascular network in radial alignment (Fig. S4 in Supplementary Information). This indicated that highly metastatic tumor cells were able to polarize and migrate in response to the growth factors and nutrients from the vasculature [32]. Moreover, by combining the tissue chamber and diverse DTBs (Fig. S5 in Supplementary Information), we constructed a versatile coculture tissue model that met the requirement for organs with specific microphysiological functions, which could further facilitate the study of tissue-to-tissue interactions.

Discussion

The organ-on-a-chip device is typically designed to simulate an in vivo-like microenvironment and interactions between different cells/tissues. Owing to the structural complexity of living tissues and organs, ECM patterning with high spatial control and reproducibility remains challenging and requires innovative fabrication methods [33]. Photopatterning methods have been used extensively for hydrogel patterning; however, they usually require a photosensitive moiety that may adversely affect cell survival. Advanced 3D bioprinting is a powerful tool that has gradually matured in additive manufacturing for tissue engineering. However, the printing process is normally performed in an open environment rather than inside a closed microfluidic chip under dynamic flow conditions. Additionally, gel patterning, which uses a driving force from external physical fields, such as electric, magnetic, and acoustic fields, typically requires specific modification of the hydrogel.

In this study, the integration of a DTB enabled robust hydrogel patterning with high spatial resolution inside closed

Fig. 11 Engineered I♡SJTU-shaped microvascular network using the DTB design. Scale bar: 500 μm. DTB: dissolvable temporary barrier

microdevices without pretreatment of the hydrogel or use of external equipment. Besides the glass substrate, the DTB could be flexibly patterned on other plastic materials (Fig. S6 in Supplementary Information), such as polymethyl methacrylate, polycarbonate, and polyvinyl chloride. Thus, DTB-embedded microfluidic chips are likely to be fabricated by hot embossing and injection molding. Furthermore, irregular DTB structures can be flexibly regulated for specific ECM patterning depending on the model requirements. The I♡SJTU-shaped vascular network shown in Fig. 11 was constructed using DTB patterns shown in Fig. S7 (Supplementary Information).

As a proof-of-concept, the DTB model still requires several improvements before it can be applied with versatility. Regarding device fabrication, the minimal height of the DTB is limited by the thickness of the stencil mask to approximately 100 μm. Extrusion-based 3D bioprinting could be used as an alternative for high-precision barrier production [34]. Nonetheless, owing to the cylindrical cross-section of the barrier, the barrier may not adequately prevent the ECM from bursting outside the tissue chamber. Additionally, multilayered DTBs having different patterns may contribute to the hierarchical microstructure of biological tissues. Although the DTB model presented is the initial prototype, programmable machines may assist in stencil printing and alignment for mass production. Apart from PVA in stencil printing, the simultaneous or sequential patterning of multimaterials, such as conductive polymers, may expand DTB application scenarios, which may promote the future commercialization of the organ-on-a-chip devices.

In disease modeling, the DTB-based microvascular system is an essential bridge for organ interconnection, and it is likely to improve the currently reported multiorgan-on-a-chip devices and vascularized tumor models in an advanced format that is free of physical barriers. The direct interconnection between vasculature and other organs may further enhance the efficiency and accuracy of pharmacodynamic–pharmacokinetic modeling. The standardization of DTB design toward multiple compartments also provides an opportunity for the study of functional barriers, such as the blood–brain barrier and epithelial and immunological barriers. Moreover, controllable fluid stimulation in the tissue chamber makes it possible to construct disease organoids from patient-derived cells, which may contribute to auxiliary clinical diagnoses and treatment in precision medicine. Therefore, based on its capacity to maintain physiological fidelity in the vascular system, DTB design could serve as a new regimen for the study of multitissue interactions as well as drug functions in organ-on-a-chip models.

Conclusions

In this study, we presented a novel, flexible DTB design that achieved robust ECM patterning and applied physiologically relevant flow stimuli to cells/tissues. The DTB was compatible with tissue chambers of different shapes, including single and multiple compartments with either straight or curved DTB structures. The effectiveness of the DTB design was validated using engineered vasculature through different vascularization mechanisms. Compared with physical barriers, both the simulation and comparative experimental results on vasculogenesis demonstrated that DTB design resulted in more interstitial flow stimuli to the ECM. We expect this method to serve as a practical paradigm for ECM patterning toward in vitro models without physical barriers, which could facilitate the development of novel organ-on-a-chip devices with a physiologically relevant microenvironment.

Supplementary Information The online version contains supplementary material available at https://doi.org/10.1007/s42242-023-00267-x.

Acknowledgements This work was supported by the National Natural Science Foundation of China (Nos. 31972929 and 62231025), the Research Program of Shanghai Science and Technology Committee (Nos. 21140901300 and 20DZ2220400), the Natural Science Foundation of Chongqing, China (No. CSTB2022NSCQ-MSX0767), the Interdisciplinary Program of Shanghai Jiao Tong University (Nos. YG2021ZD22 and YG2023LC04), the Foundation of National Center for Translational Medicine (Shanghai) SHU Branch (No. SUITM-2023008), and the Cross-disciplinary Research Fund of Shanghai Ninth People's Hospital, Shanghai Jiao Tong University School of Medicine (No. JYJC202108). The authors were also grateful to the Center for Advanced Electronic Materials and Devices (AEMD) of Shanghai Jiao Tong University.

Author contributions DW and QYL were involved in conceptualization, investigation, methodology, writing—original draft, and visualization; CYZ, ZJL, KYL, YJL, and LX helped in resources and writing—review and editing; XLW contributed to supervision and funding acquisition.

Declarations

Conflict of interest The authors declare that they have no conflict of interest.

Ethical approval This article does not contain any studies with human or animal subjects performed by any of the authors.

References

1. Bhatia SN, Ingber DE (2014) Microfluidic organs-on-chips. Nat Biotechnol 32(8):760–772. https://doi.org/10.1038/nbt.2989
2. Chan CY, Huang PH, Guo F et al (2013) Accelerating drug discovery via organs-on-chips. Lab Chip 13(24):4697–4710. https://doi.org/10.1039/c3lc90115g
3. Low LA, Tagle DA (2017) Tissue chips–innovative tools for drug development and disease modeling. Lab Chip 17(18):326–336. https://doi.org/10.1039/c7lc00462a
4. Van De Stolpe A, Den Toonder J (2013) Workshop meeting report organs-on-chips: human disease models. Lab Chip 13(18):3449–3470. https://doi.org/10.1039/c3lc50248a
5. Wang X, Sun Q, Pei J (2018) Microfluidic-based 3D engineered microvascular networks and their applications in vascularized microtumor models. Micromachines 9(10):493. https://doi.org/10.3390/mi9100493
6. Kim S, Lee H, Chung M et al (2013) Engineering of functional, perfusable 3D microvascular networks on a chip. Lab Chip 13(8):1489–1500. https://doi.org/10.1039/c3lc41320a
7. Zheng Y, Chen JM, Craven M et al (2012) In vitro microvessels for the study of angiogenesis and thrombosis. Proc Natl Acad Sci USA 109(24):9342–9347. https://doi.org/10.1073/pnas.1201240109
8. Li QY, Niu K, Wang D et al (2022) Low-cost rapid prototyping and assembly of an open microfluidic device for a 3D vascularized organ-on-a-chip. Lab Chip 22(14):2682–2694. https://doi.org/10.1039/d1lc00767j
9. Hsu YH, Moya ML, Abiri P et al (2013) Full range physiological mass transport control in 3D tissue cultures. Lab Chip 13(1):81–89. https://doi.org/10.1039/c2lc40787f
10. Chen MB, Whisler JA, Jeon JS et al (2013) Mechanisms of tumor cell extravasation in an in vitro microvascular network platform. Integr Biol 5(10):1262–1271. https://doi.org/10.1039/c3ib40149a
11. Yeon JH, Ryu HR, Chung M et al (2012) In vitro formation and characterization of a perfusable three-dimensional tubular capillary network in microfluidic devices. Lab Chip 12(16):2815–2822. https://doi.org/10.1039/c2lc40131b
12. Vulto P, Podszun S, Meyer P et al (2011) Phaseguides: a paradigm shift in microfluidic priming and emptying. Lab Chip 11(9):1596–1602. https://doi.org/10.1039/c0lc00643b
13. Trietsch SJ, Israëls GD, Joore J et al (2013) Microfluidic titer plate for stratified 3D cell culture. Lab Chip 13(18):3548–3554. https://doi.org/10.1039/c3lc50210d
14. Wang XL, Phan DTT, Sobrino A et al (2016) Engineering anastomosis between living capillary networks and endothelial cell-lined microfluidic channels. Lab Chip 16(2):282–290. https://doi.org/10.1039/c5lc01050k
15. Cho H, Kim HY, Kang JY et al (2007) How the capillary burst microvalve works. J Colloid Interface Sci 306(2):379–385. https://doi.org/10.1016/j.jcis.2006.10.077
16. Wong AP, Perez-Castillejos R, Christopher Love J et al (2008) Partitioning microfluidic channels with hydrogel to construct tunable 3-D cellular microenvironments. Biomaterials 29(12):1853–1861. https://doi.org/10.1016/j.biomaterials.2007.12.044
17. Loessberg-Zahl J, Beumer J, van den Berg A et al (2020) Patterning biological gels for 3D cell culture inside microfluidic devices by local surface modification through laminar flow patterning. Micromachines 11(12):1112. https://doi.org/10.3390/mi11121112
18. Yamada A, Renault R, Chikina A et al (2016) Transient microfluidic compartmentalization using actionable microfilaments for biochemical assays, cell culture and organs-on-chip. Lab Chip 16(24):4691–4701. https://doi.org/10.1039/c6lc01143h
19. Tibbe MP, Leferink AM, van den Berg A et al (2018) Microfluidic gel patterning method by use of a temporary membrane for organ-on-chip applications. Adv Mater Technol 3(3):1700200. https://doi.org/10.1002/admt.201700200
20. Pei JH, Sun QY, Yi ZR et al (2020) Recoverable elastic barrier for robust hydrogel patterning with uniform flow profile for organ-on-a-chip applications. J Micromech Microeng 30(3):35005. https://doi.org/10.1088/1361-6439/ab68b2
21. Goldschmidtboeing F, Rabold M, Woias P (2006) Strategies for void-free liquid filling of micro cavities. J Micromech Microeng 16(7):1321–1330. https://doi.org/10.1088/0960-1317/16/7/029
22. Chibbaro S, Costa E, Dimitrov DI et al (2009) Capillary filling in microchannels with wall corrugations: a comparative study of the Concus−Finn criterion by continuum, kinetic, and atomistic approaches. Langmuir 25(21):12653–12660. https://doi.org/10.1021/la901993r
23. Wang XL, Phan DTT, Zhao D et al (2016) An on-chip microfluidic pressure regulator that facilitates reproducible loading of cells and hydrogels into microphysiological system platforms. Lab Chip 16(5):868–876. https://doi.org/10.1039/c5lc01563d
24. Sobrino A, Phan DTT, Datta R et al (2016) 3D microtumors in vitro supported by perfused vascular networks. Sci Rep 6(1):31589. https://doi.org/10.1038/srep31589
25. Phan DTT, Wang XL, Craver BM et al (2017) A vascularized and perfused organ-on-a-chip platform for large-scale drug screening applications. Lab Chip 17(3):511–520. https://doi.org/10.1039/c6lc01422d
26. Li S, Butler P, Wang YX et al (2002) The role of the dynamics of focal adhesion kinase in the mechanotaxis of endothelial cells. Proc Natl Acad Sci USA 99(6):3546–3551. https://doi.org/10.1073/pnas.052018099
27. Laco F, Grant MH, Black RA (2013) Collagen-nanofiber hydrogel composites promote contact guidance of human lymphatic microvascular endothelial cells and directed capillary tube formation. J Biomed Mater Res A 101A(6):1787–1799. https://doi.org/10.1002/jbm.a.34468
28. Ivanov KP, Kalinina MK, Levkovich YI (1981) Blood flow velocity in capillaries of brain and muscles and its physiological significance. Microvasc Res 22(2):143–155. https://doi.org/10.1016/0026-2862(81)90084-4
29. Patan S (2004) Vasculogenesis and angiogenesis. Cancer Treat Res 117:3–32. https://doi.org/10.1007/978-1-4419-8871-3_1
30. Kim SD, Chung M, Ahn J et al (2016) Interstitial flow regulates the angiogenic response and phenotype of endothelial cells in a 3D culture model. Lab Chip 16(21):4189–4199. https://doi.org/10.1039/c6lc00910g
31. Nashimoto Y, Hayashi T, Kunita I et al (2017) Integrating perfusable vascular networks with a three-dimensional tissue in a microfluidic device. Integr Biol 9(6):506–518. https://doi.org/10.1039/c7ib00024c
32. Bockhorn M, Jain RK, Munn LL (2007) Active versus passive mechanisms in metastasis: do cancer cells crawl into vessels, or are they pushed? Lancet Oncol 8(5):444–448. https://doi.org/10.1016/S1470-2045(07)70140-7
33. Primo GA, Mata A (2021) 3D patterning within hydrogels for the recreation of functional biological environments. Adv Funct Mater 31(16):2009574. https://doi.org/10.1002/adfm.202009574

34. Miri AK, Mirzaee I, Hassan S et al (2019) Effective bioprinting resolution in tissue model fabrication. Lab Chip 19(11):219–237. https://doi.org/10.1039/c8lc01037d

Authors and Affiliations

Ding Wang[1] · Qinyu Li[2] · Chenyang Zhou[1] · Zhangjie Li[1] · Kangyi Lu[1] · Yijun Liu[1] · Lian Xuan[3] · Xiaolin Wang[1,3,4,5]

✉ Xiaolin Wang
xlwang83@sjtu.edu.cn

[1] Department of Micro/Nano Electronics, School of Electronic Information and Electrical Engineering, Shanghai Jiao Tong University, Shanghai 200240, China

[2] Department of Ophthalmology, LKS Faculty of Medicine, The University of Hong Kong, Hong Kong 999077, China

[3] Institute of Medical Robotics, Shanghai Jiao Tong University, Shanghai 200240, China

[4] National Key Laboratory of Advanced Micro and Nano Manufacture Technology, Shanghai Jiao Tong University, Shanghai 200240, China

[5] National Center for Translational Medicine (Shanghai) SHU Branch, Shanghai University, Shanghai 200444, China